Structure and Dynamics of 1-Ethyl-3-methylimidazolium Acetate via Molecular Dynamics and Neutron Diffraction

D. T. Bowron,[†] C. D'Agostino,[‡] L. F. Gladden,[‡] C. Hardacre,*,[§] J. D. Holbrey,[§] M. C. Lagunas,[§] J. McGregor,[‡] M. D. Mantle,[‡] C. L. Mullan,[§] and T. G. A. Youngs[§]

Rutherford Appleton Laboratory, Chilton, Didcot, Oxon, OX11 0QX, U.K., Department of Chemical Engineering and Biotechnology, University of Cambridge, Cambridge CB2 3RA, U.K., and School of Chemistry and Chemical Engineering/School of Mathematics and Physics, The QUILL Centre, Queen's University Belfast, Belfast BT9 5AG, U.K.
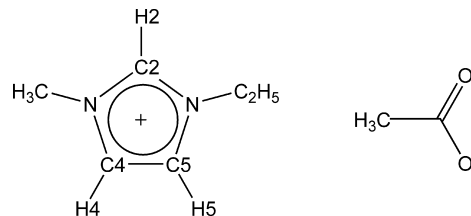
The liquid state structure of the ionic liquid, 1-ethyl-3-methylimidazolium acetate ([C$_2$mim][OAc]), an excellent nonderivitizing solvent for cellulosic biomass, has been investigated at 323 K by molecular dynamics (MD) simulation and by neutron diffraction using the SANDALS diffractometer at ISIS to provide experimental differential neutron scattering cross sections from H/D isotopically substituted materials. Ion−ion radial distribution functions both calculated from MD and derived from the empirical potential structure refinement (EPSR) model to the experimental data show the alternating shell structure of anions around the cation, as anticipated. Spatial probability distributions reveal the main anion-to-cation features as in-plane interactions of anions with the three imidazolium ring hydrogens and cation−cation planar stacking above/below the imidazolium rings. Interestingly, the presence of the polarized hydrogen-bond acceptor (HBA) anion (acetate) leads to an increase in anion−anion tail−tail structuring within each anion shell, an indicator of the onset of hydrophobic regions within the anion regions of the liquid. MD simulations show the importance of scaling of the effective ionic charges in the basic simulation approach to accurately reproduce both the observed experimental neutron scattering cross sections and ion self-diffusion coefficients.

Introduction

The structure of ionic liquids is dominated by the Coulombic ion−ion lattice interactions combined with rotational and/or torsional fluxionality of ions which helps inhibit efficient packing of ions and gives a net reduction in lattice energies. These two interactions give rise to the basic liquid structure of ionic liquids (and higher temperature molten salts) comprised of alternating shells of ions in which each cation is surrounded by anions and vice versa, with the structural correlation extending out to the second or third shell.

The role of specific atomic features of ionic liquid ions providing secondary structure-directing features in the liquid state is well established and predominantly manifests itself as hydrogen bonding interactions. In this case, weakly acidic hydrogen atoms serve as the H-bond donors, typically those aromatic hydrogens present in the C−H bonds of the imidazolium ring. Until now, the most widely studied anions have been simple (pseudo-) spherical ions with no (e.g., halides) or highly symmetrical directional interactions (e.g., [PF$_6$]$^-$). Other anions in common usage and whose structure has been studied include bis{(trifluoromethyl)sulfonyl}imide ([NTf$_2$]$^-$) which is large, highly flexible, and at the same time weakly coordinating. The acetate ([OAc]$^-$) anion in the ionic liquid of the present study is, by contrast, small and polar, possessing a hydrophobic methyl tail together with a hydrophilic carboxylate headgroup. In

Figure 1. Structure of 1-ethyl-3-methylimidazolium acetate, identifying the nomenclature of the ionic liquid cation.

addition to the directionality this imposes on the interaction between cation and anion, the carboxylate headgroup is also bidentate.

Interest in ionic liquids with acetate anions stems from the first report of the dissolution of cellulose in 1-alkyl-3-methylimidazolium chloride ionic liquids[1] and the subsequent explosion of interest[2] in the application of ionic liquids in biomass processing to access or generate polymeric materials[3] and energy products[4] (HMF, fermentable sugars, etc.). The search for other ionic liquid classes that could also dissolve polysaccharides has yielded two anions that appear to provide comparable solubilizing characteristics, dimethylphosphate[5] and acetate (both coupled with small imidazolium cations). 1-Ethyl-3-methylimidazolium ([C$_2$mim][OAc]) (Figure 1) is perhaps the "best" cellulosic solvent identified[6] and, additionally, also shows useful enzyme[7] and environmentally friendly characteristics and significant ability to capture CO$_2$.[8] [C$_2$mim][OAc] has been probed utilizing vibrational spectroscopy and also the effect of dissolution of glucose/cellobiose in the ionic liquid.[9]

Given the interest in this ionic liquid, and the differences in anion structure from that of the simple halides, as mentioned

---

* Corresponding author. E-mail: c.hardacre@qub.ac.uk.
† Rutherford Appleton Laboratory.
‡ University of Cambridge.
§ Queen's University Belfast.

Structure and Dynamics of [C₂mim][OAc]

J. Phys. Chem. B, Vol. 114, No. 23, 2010 **7761**

above, an investigation of both the ionic liquid structure and the solvation structure of glucose in [C$_2$mim][OAc] was undertaken. Initially, we report the structure of the neat ionic liquid system, and results from the solvated structure of glucose in the ionic liquid will be reported in due course. A comparison with the corresponding studies on 1,3-dimethylimidazolium chloride and 1,3-dimethylimidazolium chloride/glucose solvation structures provides valuable insight into the role of the ionic liquid components in cellulose dissolution, as well as, more fundamentally, the influences of the secondary structure interactions on the overall structure of ionic liquids, in general.

Herein, we describe the liquid structure of [C$_2$mim][OAc] derived from isotopic contrast neutron scattering experiments with that obtained independently using a classical MD simulation approach. Cation and anion self-diffusion constants have been calculated by MD and are compared with experimental data determined by pulsed field gradient (PFG) NMR spectroscopy.

Experimental Section

Neutron scattering data were collected at the ISIS pulsed neutron and muon source at Rutherford Appleton Laboratory, UK, using the SANDALS instrument. The instrument has a wavelength range of 0.05−4.5 Å, and data were collected over the Q range 0.1−50 Å^{-1}. Each sample was contained in null scattering Ti$_{0.68}$Zr$_{0.32}$ flat plate cells of internal geometry of 1 × 35 × 35 mm with a wall thickness of 1 mm. During the measurements, the cell was maintained at a temperature of 323 K using a Julabo circulating heater. Measurements were made on each of the empty sample holders, the empty spectrometer, and a 3.1 mm thick vanadium standard sample for the purposes of instrument calibration and data normalization. After appropriate normalization for the cell and the window material, good reproducibility was found between the sample cells. Data analysis was performed using GUDRUN, based upon algorithms in the ATLAS package,[10] to produce a differential scattering cross section for each sample. The experimental sample densities and scattering levels were consistent with the correct isotopic compositions of the samples. Calibration and background subtraction for single atom scattering was made to produce an interference differential scattering cross section for each sample.

Four 1-ethyl-3-methylimidazolium acetate ionic liquids containing protiated and deuterated cations and anions were prepared and analyzed using ^{1}H NMR and electrospray mass spectrometry (ES-MS). Ionic liquids with protiated cations were synthesized by alkylation of methylimidazole with diethylsulfate[11] followed by anion hydrolysis and anion exchange via hydroxide to acetate using appropriately deuteriated or protiated acetic acid. The two ionic liquids with perdeuteriated cations were synthesized by alkylation of methylimidazole-d_6 with bromoethane-d_5 followed by anion metathesis, first to hydrogen sulfate and then to acetate as above with protiated or perdeuteriated acetic acid. The hygroscopic ionic liquids were dried at 50 °C under high vacuum until constant mass was obtained (typically 6 h) and then stored under dry nitrogen until transfer to the spectrometer. Higher temperatures were avoided to prevent sample decomposition.

Neutron scattering data were collected for seven samples with a range of hydrogen isotope substitutions, namely, fully protiated and fully deuteriated 1-ethyl-3-methylimidazolium acetate, ILs with perdeuteriated cation, perdeuteriated anion, and three samples containing 1:1 mixtures of protiated and perdeuteriated cation, cation and anion, and anion.

The neutron diffraction data were analyzed using the empirical potential structure refinement (EPSR) approach.[12] This
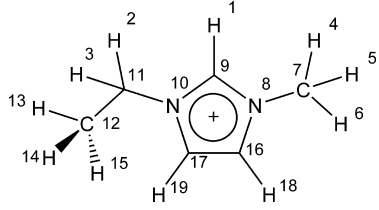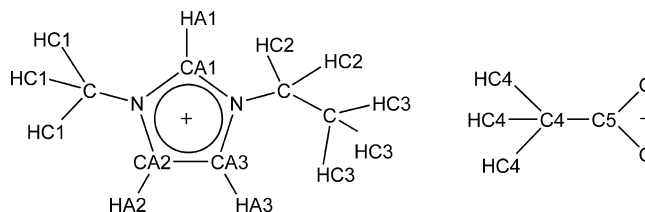

Figure 2. Atom types of the [C$_2$mim]$^+$ cation and [OAc]$^-$ anion used in the EPSR model.

TABLE 1: Lennard-Jones, Charge, and Atomic Mass Parameters Used for the Reference Potential of the Empirical Potential Structure Refinement Model of 1-Ethyl-3-methylimidazolium Acetate
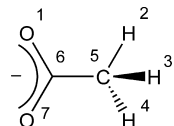
atom	ε (kJ mol^{-1})	σ (Å)	q (e)
HA1	0.200	2.40	0.210
HC2	0.200	2.50	0.013
HC1	0.200	2.50	0.130
C	0.500	3.50	−0.130
N	0.500	3.25	0.150
CA1	0.500	3.50	−0.110
HC3	0.200	2.50	0.060
CA2	0.500	3.50	−0.130
HA2	0.200	2.40	0.210
HA3	0.200	2.40	0.210
O	0.655	3.17	−0.800
HC4	0.200	2.50	0.060
C4	0.500	3.50	−0.280
C5	0.500	3.50	0.700

refinement consists of a Monte Carlo simulation using Lennard-Jones potentials with atom-centered point charges comparing the residuals from the simulated data with experimental in Q-space. The modeling process combines this data with basic information about the structure of the ions and total atomic densities of the system to constrain the model in a chemically and physically reliable manner. The experimental total structure factor $F(Q)$ extracted from the neutron scattering data for each of the four samples was used to build and refine a three-dimensional model of the liquid structure consistent with the experimental data using EPSR. The EPSR refinement was initialized using an equilibrated Monte Carlo simulation of 200 ion pairs in a cubic box of dimension 37.325 Å at 323 K, corresponding to an atomic density of 0.1 atoms Å^{-3} equivalent to the experimentally determined molecular density of the fully protiated ionic liquid. The selective ^{1}H and ^{2}H substitution on the cation and anion provided seven data sets which were compared with the simulation, thus increasing the confidence in the EPSR-derived structure. Partial radial distribution functions describing the distributions of cations and anions around a central cation or anion were calculated using the SHARM routines within EPSR using the anion center of mass and cation center of mass of the imidazolium ring as positions of reference.

Atom types were defined based on their unique positions in the molecular skeleton of the two ions, as shown in Figure 2. The full parameters of the reference potential used, derived from OPLS-AA parameters with charges scaled by 0.8 (see Discussion), are given in Table 1. Tables 2 and 3 summarize the interatomic distance constraints used to define the basic molecular geometry of the cation and anion, respectively, within the model. The distance constraints for the ionic liquid ions were obtained from the averaged atomic coordinates in the single crystals of 1-ethyl-3-methylimidazolium salts and from ab initio minimized geometry of the acetate anion using GAMESS-US[13] at the MP2/6-31G(d) level of theory.

TABLE 2: Intramolecular Distance Constraints Used to Define the Basic Structure of the 1-Ethyl-3-methylimidazolium Cation with Atom Numbering Corresponding to the Atom Types in the Initial EPSR Simulation Model

atom type	d (Å)	1	2	3	4	5	6	7	8	9	10	11	12	13	14	15	16	17	18	19
HA1	1								2.2	1.09	2.2									
HC2	2			1.81							2.13	1.11	2.18							
HC2	3										2.13	1.11	2.18							
HC1	4					1.81	1.81	1.11	2.13											
HC1	5						1.81	1.11	2.13											
HC1	6							1.11	2.13											
C	7								1.49	2.56							2.58			
N	8									1.38	2.24						1.41	2.25	2.2	
CA1	9										1.38	2.56					2.26	2.26		
N	10											1.49	2.47				2.25	1.41		2.2
C	11												1.54	2.18	2.18	2.18	2.58			
C	12													1.11	1.11	1.11				
HC3	13														1.81	1.81				
HC3	14															1.81				
HC3	15																			
CA2	16																	1.38	1.09	2.25
CA2	17																		2.25	1.09
HA2	18																			
HA3	19																			

TABLE 3: Intramolecular Distance Constraints Used to Define the Basic Structure of the Acetate Anion with Atom Numbering Corresponding to the Atom Types in the Initial EPSR Simulation

atom type	d (Å)	1	2	3	4	5	6	7
O	1					2.41	1.26	2.22
HC4	2			1.78	1.78	1.11	2.22	
HC4	3				1.78	1.11	2.22	
HC4	4					1.11	2.22	
C4	5						1.55	2.41
C5	6							1.26
O	7							

All the PFG NMR experiments were carried out on a Bruker Biospin DMX 300 spectrometer, operating at a ^{1}H frequency of 300.13 MHz, equipped with a diffusion probe capable of producing magnetic field gradient strength pulses up to 11.6 T m^{-1}. The measurements were performed at variable temperature from 293 to 323 K, with increments of 5 K to an accuracy of ±0.1 K. A Bruker digital variable temperature unit, BVT 3000, was used to set the required temperature for each experiment. Samples were prepared in 5 mm NMR tubes and filled to a vertical height of approximately 40 mm. For each temperature, the sample was left for 15 min before starting the measurement, to reach thermal equilibrium. Diffusion measurements were carried out using a standard PGSTE pulse sequence.[14] Sixteen spectra were acquired per sample with the gradient strength being varied between 0.05 and 10 T m^{-1}. The observation time, Δ, was set to 50 ms. Typical values of δ were 3 and 3.5 ms. The numerical values of the diffusion coefficient, D, were obtained by fitting the NMR signal decay function to the following expression

$$E = \exp\left[-D\gamma^2 g^2 \delta^2\left(\Delta - \frac{\delta}{3}\right)\right]$$

where γ is the gyromagnetic ratio of the nuclei being studied (i.e., ^{1}H in our case) and E is the measured signal/spectral intensity.

Computational Details. All simulations were performed with the DL_POLY software.[15] For the preliminary bulk system, simulation random initial configuration of 200 ion pairs of the liquid in a cubic box was generated at the experimental liquid density of 1.086 g cm^{-3} (1.00 atoms Å^{-3}) at 323 K and subjected to initial relaxation runs at short time steps (ranging from 10^{-8} to 10^{-4} ps). Simulations of 500 ps at the target time step of 10^{-3} ps were made and discarded ahead of the main data collection run. The NVT ensemble was employed with a thermostat relaxation time of 0.1 ps, while short-range interactions were truncated at 15.0 Å, as were real-space interactions in the Ewald sum ($\alpha = 0.23833$, $k = 16$). The [C$_2$mim]$^+$ cation was represented by the forcefield of Canongia-Lopes and Padua,[16] while parameters for the [OAc]$^-$ anion were taken directly from OPLS-AA and used without modification,[17] except for the application of C–H bond constraints in line with the larger time step employed. Cross-terms were generated with the Lorentz–Bertholet combination rules, and the 1,4-interactions were scaled by 0.5. The main production run spanned 6 ns of simulation time, and all properties were calculated over the last 3 ns of this period. For the charge-scaled simulation systems, either 50 or 200 ion pairs were run in the NPT ensemble with relaxation times for the thermostat and barostat of 0.2 and 0.1 ps, respectively. Interaction cutoffs were adjusted to suit, in the case of the smaller system.
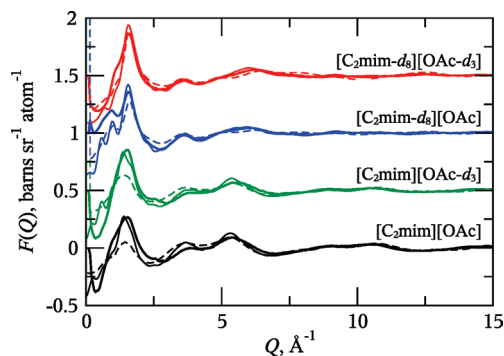
Figure 3. Total scattering profiles measured by neutron diffraction (thick solid lines), the fits to these data from EPSR (thin solid lines), and those calculated from molecular dynamics (dashed lines) as a function of Q for 1-ethyl-3-methylimidazolium acetate at 323 K.
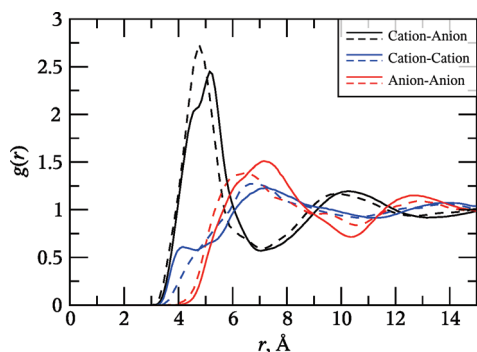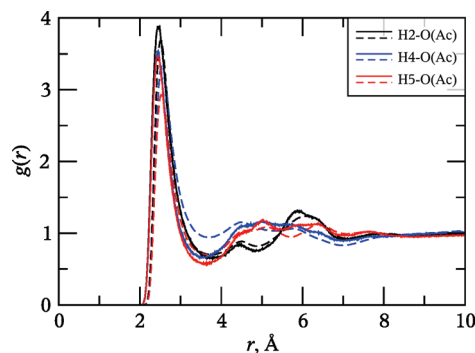

Figure 4. Comparison of the radial distribution functions for the cation—anion distribution (black line), the cation—cation distribution (blue line), and the anion—anion distribution (red line) for 1-ethyl-3-methylimidazolium acetate at 323 K determined from molecular dynamics simulation (solid lines) and EPSR analysis of experimental neutron scattering data (dashed lines). For the anion, the center of mass is used, while for the cation the midpoint of the N—N vector of the imidazolium ring is employed.

Results and Discussion

Previously, we have performed neutron diffraction studies on 1,3-dialkylimidazolium ionic liquids containing simple spherical or noncoordinating anions such as Cl⁻,[18] [PF₆]⁻,[19] and [NTf₂]⁻,[20] and the general picture of an individual ion being surrounded by a shell of ~7 oppositely charged species holds across all three ionic liquids. The spherical shape of the Cl⁻ and [PF₆]⁻ anions allows the anion to interact with equally strong hydrogen bonds to more than one cation, but in the present work this key property of the anion has been removed to a large extent. Figure 3 shows the measured total scattering profiles for the four isotopically substituted pure liquid samples, along with the refined EPSR fits and those calculated from the MD simulation. Overall, aside from some minor discrepancies in the low-Q region, the EPSR fits to the data are good, as is the agreement between the EPSR and MD results.

Figure 4 shows the ion—ion radial distribution functions (RDFs) between ions, calculated from the MD simulation (solid lines) and from the EPSR analysis of neutron data (dashed lines). The average cation—cation and cation—anion separations at ~7 and ~5 Å, respectively, are comparable with those found for other ionic liquids.[18−20] The first peak in the cation—anion RDF is noticeably broader than that observed for 1,3-dimethylimidazolium chloride[18] and bears more resemblance to [C₁mim][NTf₂],[20] as is also the case for [C₄mim][CF₃COO].[21] The typical features expected for these systems are found: alternating, out-of-phase distributions of one ion around another


Figure 5. Comparison of the site—site partial radial distribution functions for the [C₂mim]⁺ ring hydrogens to the acetate oxygens for 1-ethyl-3-methylimidazolium acetate at 323 K derived from molecular dynamics simulation (solid lines) and EPSR analysis of experimental neutron scattering data (dashed lines).

and, as is the case for other imidazolium-based ionic liquids containing Cl⁻ and [PF₆]⁻ anions, very little encroachment of like-ions into the primary coordination shell of each ion. The peak at ~4 Å (MD) and small shoulder at ~5 Å (EPSR) in the cation—cation curve is indicative of ring-stacking and depends strongly on the nature of the anion—such features may be found in simulations of, for example, [C₁mim]Cl and in the solution-state ¹H NMR spectra of [C₂mim]Cl.[22] The magnitude of cation—cation stacking decreases markedly on increasing the size and reducing coordinating ability of the anion present so that some evidence of weak, low probability stacking is observed for [C₁mim][PF₆][19] but not [C₁mim][NTf₂],[20] as the reduced positionally defined anion—cation interactions led to a more isotropic distribution of anions around cations.[23] Analysis of cation vectors normal to the plane of the ring for cation pairs within this distance shows a heavy bias toward a near-planar orientation with a slight tilt of the order of 10−20°. Furthermore, these data show that the configuration of the near-planar interaction where the two cations are oriented with ethyl chains "top to tail" is preferred over the side-by-side case. This orientation of ethyl groups is most likely driven by steric packing factors. The first peak in the cation—anion distribution is broader than is the case for spherical anions and bears more similarity to those found for [NTf₂]⁻ systems, despite the [NTf₂]⁻ being much larger and more diffuse than the acetate, which indicates that the shell of anions around each cation is significantly thicker than the length of the acetate anion. This implies, and is supported (see later), that the anions form an approximate bilayer structure with charged carboxylate groups oriented toward cations in each adjacent shell and hydrophobic methyl groups in a central domain. Integration of the cation—anion RDF up to the first minimum at 7 Å gives a coordination number of 6.9, which is comparable with that obtained from EPSR fitting to the neutron diffraction data (6.8) and also to those found for other ionic liquid systems. The RDFs derived from EPSR analysis of the neutron diffraction data and those of the MD show good agreement save for the prepeak at 4 Å in the cation—cation correlation which is less pronounced in the EPSR data. Possible explanations for this may lie either with the MD, for which the cation—cation interaction may be overly favored, or in the EPSR simulation, in which the increased flexibility of the molecules may prevent such geometries from persisting.

The atom-specific partial radial distribution functions derived from EPSR relating to cation-to-anion association are shown in Figure 5 and reveal the presence of first-shell close contacts at ~2.5 Å between cation ring hydrogens and acetate oxygen atoms. This is significantly shorter than the average center of
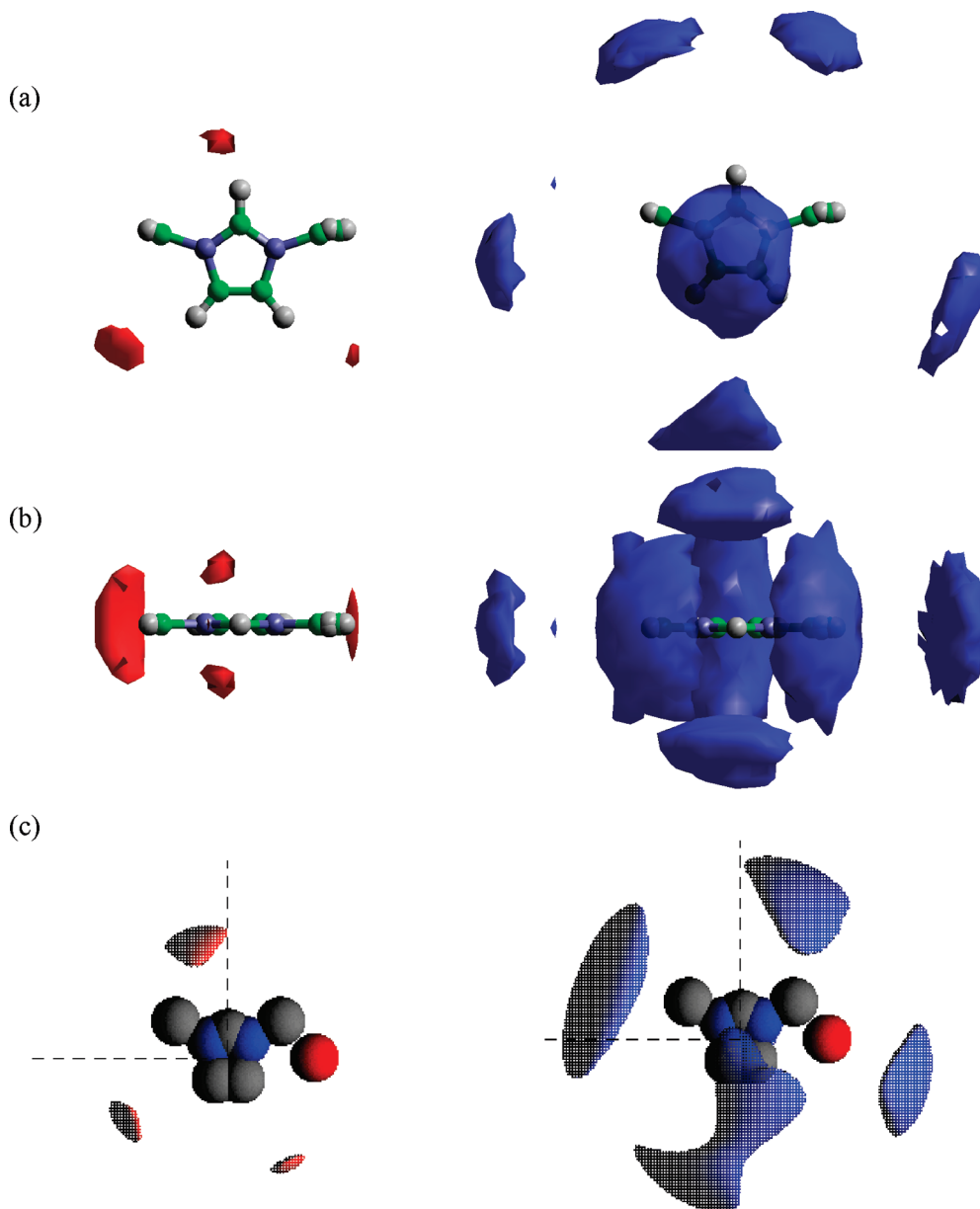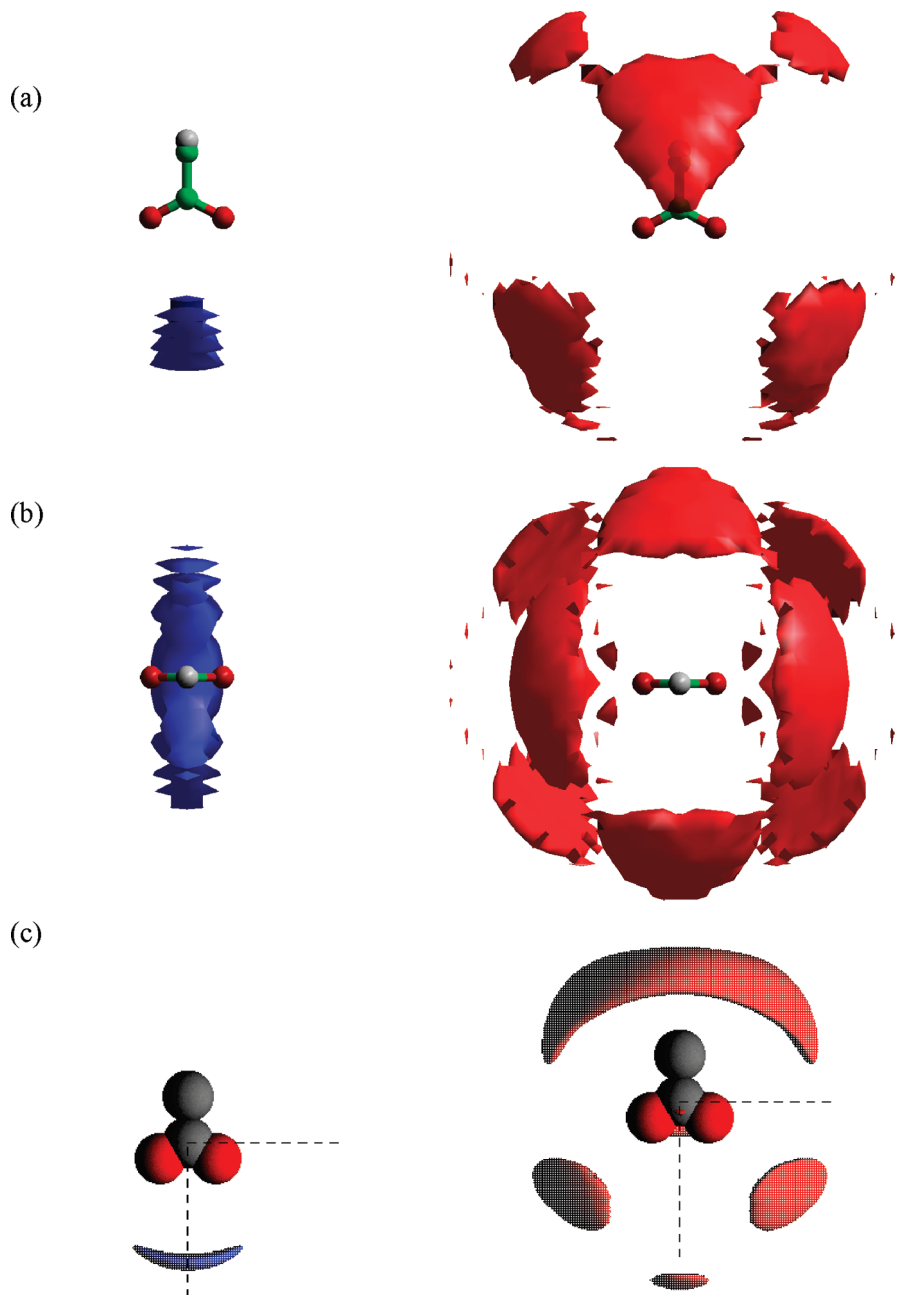
Figure 6. Probability densities of anions (red surfaces) and cations (blue surfaces) around a central cation in 1-ethyl-3-methylimidazolium acetate at 323 K calculated through MD simulation (a and b) and via EPSR (c). Surfaces are drawn to encompass the top 5% of ions within a distance corresponding to the position of the first minimum in the respective RDFs (Figure 3).

mass of cation−anion separation and suggests these are the strongest cation−anion interactions which, hence, dominate local ordering of the first shell of anions around a central cation, as expected.

Spatial probability distributions of anions within 7.4 Å (the first minimum in the cation−anion RDF) of a central cation are shown in Figure 6. Similarly to those observed previously for other ionic liquid systems, the most probable positions at which to find the anions are along the aromatic C−H bond vectors of the imidazolium ring. The distribution of anions about a central cation is not symmetric about the central axis of the imidazolium ring since anisotropy exists between the regions associated to the H(4) and H(5) carbons (Figure 1) owing to the presence of the ethyl side chain. Free rotation of the ethyl group hinders access of anions over the H(5) position, and the density is skewed toward the H(4) hydrogen of the cation. The anion density associated with the H(2) position is also offset toward the methyl group of the imidazolium cation for the same reason. This effect is more pronounced in the spherical harmonic

plots derived from the neutron scattering data. Directly above and below the cation ring plane are the most likely places to find other cations, but there also exists a regular placement of other cations around the central one, with distinct lobes present in Figure 6. The two regions located near the H(2) position are commonly observed, e.g., in [C_1mim][NTf$_2$] or [C_1mim]Cl, as is the strip associated with the H(4) and H(5) atoms of the cation. Lobes to the left and right of the alkyl chains are similar to those observed in [C_1mim]Cl[19] but in contrast with those in [C_1mim][NTf$_2$][20] which are split into two, located in the same positions in the *xy* plane but situated below and above the ring plane.

The distributions of anions and cations around a central anion (Figure 7) show first that cations are predominantly found below the bidentate jaws of the anion. Only at lower probabilities (ca. top 20% of molecules) do regions appear elsewhere toward the sides of the anion. A structural feature not observed in previous studies with ionic liquids containing Cl$^-$, [PF$_6$]$^-$, or [NTf$_2$]$^-$ anions is evident in the distribution of the acetate anions around

Figure 7. Probability densities of cations (blue surfaces) and anions (red surfaces) around a central anion in 1-ethyl-3-methylimidazolium acetate at 323 K calculated through MD simulation (a and b) and via EPSR (c). Surfaces are drawn to encompass the top 5% of ions within a distance corresponding to the position of the first minimum in the respective RDFs (Figure 3).
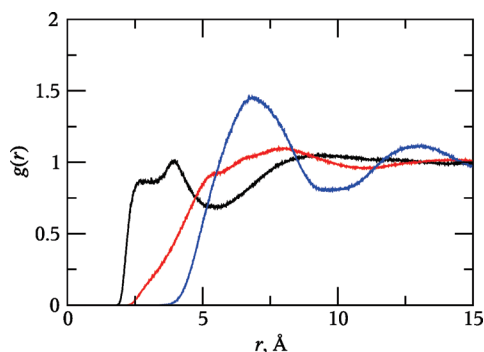
Figure 8. Partial RDFs between atom types on the [OAc] anion as calculated from MD simulation for H···H (black line), O···H (red line), and O···O (blue line).

a central anion. A strong correlation of anion CH$_3$-groups is observed which indicates a significant self-structuring. To probe the anion–anion interactions in more detail, atom–atom RDFs between acetate anions have been determined (Figure 8). The H···H partial RDF is found to have the most structure at short contact distances and, despite the maximum being slightly less than the average bulk density probability, nevertheless indicates a significant interaction, particularly because of the natural self-repulsion that a pair of small anions may be assumed to exhibit. The contact distance is also shorter than the average anion separations suggesting that these are the strongest anion–anion interactions.

A consequence of this high probability of acetate anions forming close contacts with the cation through presumably C–H···O hydrogen bonding is that tail-to-tail anion domains are formed as an outcome of the polarized HBA character of

(a)

(b)
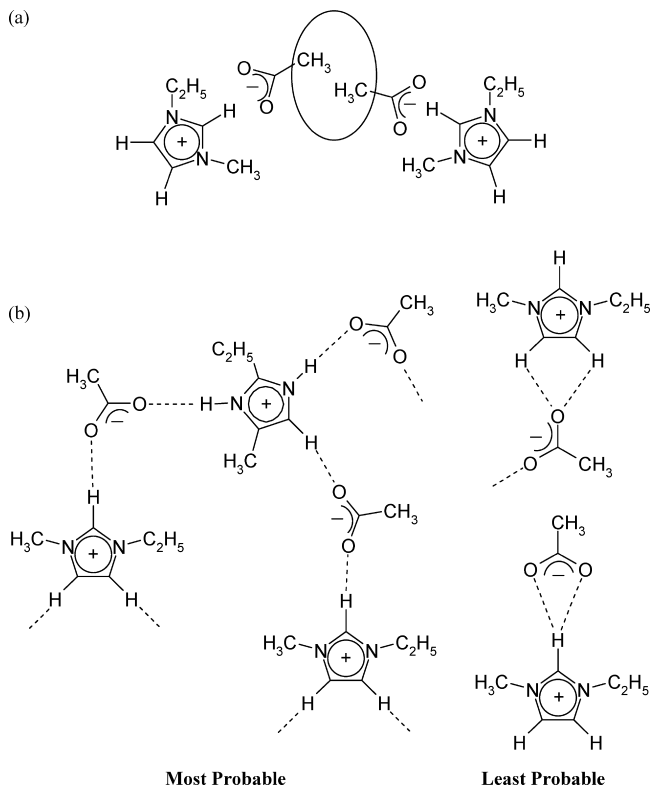
Figure 9. (a) Schematic of possible coordination in the first shell between 1-ethyl-3-methylimidazolium cations and acetate anions, with the dashed ellipse highlighting the close contacts between acetate methyl groups. (b) Schematic of coordination between 1-ethyl-3-methylimidazolium cation ring hydrogens and acetate oxygens.

TABLE 4: Coordination Numbers of Acetate Oxygens around Cation Ring Hydrogens for 1-Ethyl-3-methylimidazolium Acetate at 323 K, Where C(2), C(4), and C(5) are Labeled in Figure 1

	C(2)	C(4)	C(5)
EPSR	1.15	1.10	1.00
MD	1.33	1.13	1.16

the anion within each anion shell around a cation point of reference with three acetate carboxylate groups pointing toward the central cation and three pointing away, toward cations in the adjacent (second) shell. This alternating orientation leads to an expansion of the thickness of the acetate coordination shell, as observed in the broadening of the first peak in the anion RDF, and results in the formation of a pocket of hydrophobicity in the center of the anion shell produced from the increased probability of anion methyl−methyl contacts over carboxylate−methyl contacts (Figure 9a).

The coordination numbers of acetate oxygens around cation ring hydrogens have been calculated from both EPSR and the MD simulations and are summarized in Table 4. Values of approximately 1 indicate single (not bifurcated or bidentate) ring···O(Ac) interactions as the primary coordination in the ionic liquid system, which is represented in Figure 9b. Figure 9b shows the most probable coordination found in the extended liquid structure of 1-ethyl-3-methylimidazolium acetate, with an average of one acetate oxygen for every cation ring hydrogen as determined by coordination number. To characterize the geometry of cation−anion interactions in 1-ethyl-3-methylimidazolium acetate more fully, we consider the individual contacts between acetate oxygens and ring hydrogens. The possible interaction types between acetate oxygens and cation ring hydrogens (Figure 10) include:
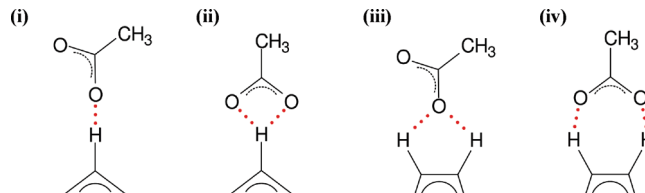
Figure 10. Possible interaction types between acetate oxygens and cation ring hydrogens include: (i) single interaction, (ii) bidentate interaction, (iii) bifurcated interaction, and (iv) bridging interaction.

TABLE 5: Number of Interactions Per Cation Per Frame with Anions in Specific Contact Configurations, Averaged Over the Three Ring Hydrogens[a]

$r(O \cdots H)_{max}$, Å	contacts %	N_{Single}	$N_{Bidentate}$	$N_{Bifurcated}$	$N_{Bridging}$	N_{Multi}
3.70	100	2.25	2.45	0.26	0.34	0.34
3.59	95	2.30	2.24	0.22	0.27	0.27
3.47	90	2.35	2.01	0.19	0.21	0.21
3.14	75	2.38	1.41	0.10	0.08	0.08

[a] Cutoff refers to the maximum allowable distance between ring H and acetate O. Interaction types are as follows: only one acetate O is close to one H and no other (H···O, single); both acetate O are close to one H and no other (O···H···O, bidentate), one acetate O is close to exactly two H (H···O···H, bifurcated); the acetate forms a bridge over two H (H···O∼O···H, bridging); and those where three or more contacts between O and H are made (multi).

(i) single interaction, where one acetate oxygen is close to one hydrogen;

(ii) bidentate interaction, where both acetate oxygens are close to one hydrogen;

(iii) bifurcated interaction, where one acetate oxygen is close to exactly two hydrogens;

(iv) bridging interaction, where acetate oxygens form a bridge over two hydrogens; and

(v) multiple interaction, where three or more contacts between oxygen and hydrogen are made.

From the acetate-O/cation-H(ring) RDF (Figure 5), we find a sharp, well-defined peak at 2.47 Å followed by a minimum at 3.7 Å. Using this value as a cutoff distance for O···H(ring) interactions (alongside other values representing the significant percentages of contacts within the larger distance), the number of instantaneous contacts formed between one or both oxygens of any acetate anion with any of the three ring hydrogens present on a single cation is analyzed. The results of this first analysis are shown in Table 5, listing the percentage of all contacts that can be grouped into the four most natural types of interaction (single, bidentate, bifurcated, and bridging geometries). It should be noted that the number of contacts are "per cation", and therefore there are half the number of bidentate anions per cation indicated in the table. We find that the H(2) position of the imidazolium ring is involved in approximately twice the number of single interactions compared with pure bidentate contacts at any given instant. This may be due to a restriction at the H(2) position due to the presence of alkyl groups on the two nitrogen atoms on either side of the cation or may be simply due to the lack of a second ring hydrogen in close proximity, as is the case for H(4) and H(5) positions. The presence of the ethyl side chain next to the H(5) hydrogen results in fewer bidentate interactions at this position and increases the probability of multicenter interactions compared with the H(4) position. A small number of bifurcated and bridging interactions are found between the H(4) and H(5) sites. This confirms that single interactions are
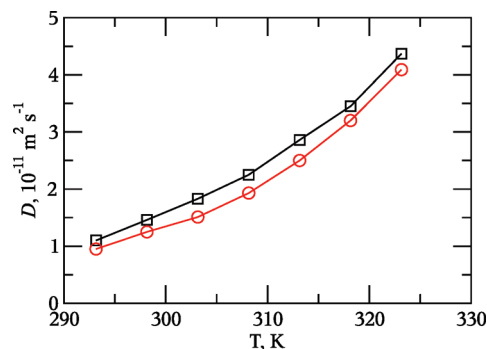
Figure 11. Temperature vs diffusion coefficient for both cations (black squares) and anions (red circles) in 1-ethyl-3-methylimidazolim acetate, obtained using PGSTE NMR.

TABLE 6: Diffusion Coefficients and Liquid Densities Calculated for Various Scaling Factors Applied to Individual Atomic Charges Where D^+ is the Cation Diffusion Coefficient and D^- Is the Anion Diffusion Coefficient

scaling factor	D^+, × 10^{-11} m^2 s^{-1}	D^-, × 10^{-11} m^2 s^{-1}	ρ, g cm^{-3}
0.70[a]	15.2		1.045
0.75[a]	14.7		1.034
0.80	9.0	6.3	1.046
0.81	6.7	4.5	1.048
0.82	6.9	4.6	1.050
0.83	6.1	3.6	1.052
0.84	4.9	3.3	1.054
0.85	4.3	2.7	1.057
0.90[a]	1.9		1.068
0.95[a]	1.74		1.076
1.00	0.80		1.088

[a] 50 ion pair simulation.

TABLE 7: Summary of the Diffusion Coefficients for the 1-Ethyl-3-methylimidazolium Cation and Acetate Anion for the Neat Ionic Liquid System Obtained from PGSTE NMR (Cambridge) Compared with Results from Moyna and Co-Workers[30] and Those Calculated from MD Simulations at 323 K

[C₂mim][OAc]	experimental D-values (m^2 s^{-1})	literature D-values (m^2 s^{-1})[32]	simulated D-values (m^2 s^{-1})
[C₂mim]$^+$	4.37×10^{-11}	4.52×10^{-11}	4.9×10^{-11}
[OAc]$^-$	4.09×10^{-11}	3.89×10^{-11}	3.3×10^{-11}

the primary contacts between cations and anions in 1-ethyl-3-methylimidazolium acetate, as indicated by the coordination number.

Stokes' law states that for a simple liquid the diffusion coefficient of a species is inversely proportional to its effective hydrodynamic radius. For noninteracting species, smaller ions will diffuse faster. However, in the case of interacting (particularly ionic) species, the effective hydrodynamic radii of the ions have the potential to be significantly increased due to association between cations and anions. Conversely, previous studies have found that cations still diffuse faster than anions, even when their corresponding effective hydrodynamic radii are calculated to be larger than those of the counterion.[24]

A number of ionic liquid diffusion coefficients have been investigated using PFG-NMR.[24−27] There have also been previous investigations of diffusion coefficients using PFG NMR for ionic liquid−solute systems.[28,29] Figure 11 shows the diffusion coefficients of the ions of 1-ethyl-3-methylimidazolium acetate as determined from pulsed-field-gradient spin−echo (PGSTE) NMR spectroscopy as a function of temperature. A cation diffusion coefficient of 4.37×10^{-11} m^2 s^{-1} and anion diffusion coefficient of 4.09×10^{-11} m^2 s^{-1} at 323 K have been obtained. These results are comparable to previous experimental measurements by Moyna et al.[30] which produce a cation diffusion coefficient of 4.52×10^{-11} m^2 s^{-1} and anion diffusion coefficient of 3.89×10^{-11} m^2 s^{-1} at 323 K.

Previous reports into the diffusion coefficients of [C₂mim]-[OAc][30] reveal that the smaller acetate ion diffuses more slowly than the imidazolium cation. The same observation has been made in this investigation to a smaller extent. The PGSTE NMR experiments showed similar D coefficients for the anions and cations in the neat ionic liquid system, despite the difference in molecular size. This has been observed previously for ionic liquids, particularly containing the tetrafluoroborate anion.[25,28,31] The cationic and anionic radii would suggest that if the Stokes−Einstein equation applies the measured cationic and anionic diffusion coefficients should differ. This implies that the ions in these ionic liquids do not diffuse as single ions but with a degree of ion pairing, that is, concerted motion rather than ion-hopping.

The MD simulations reproduce the experimental multiple scattering profiles from the isotopically substituted ionic liquids measured, and so we were interested to determine how well the simulation model could fit other macroscopic dynamical experimental data, for example, the self-diffusion coefficients of the ions. From analysis of the linear regime of the mean squared displacement (MSD) of the ions in the system, we obtain a calculated cation diffusion coefficient of 0.80×10^{-11} m^2 s^{-1}

at 323 K, while experimental measurements by Moyna et al.[30] and from our work produce a value of ∼4.5 × 10^{-11} m^2 s^{-1}, almost 1 order of magnitude larger. To address this shortcoming of the model, we have investigated scaling of the total charges on each ion in a manner similar to that performed previously for [C₁mim]Cl.[32] Table 6 shows the diffusion coefficients calculated from simulations where the individual charges on the ions have been scaled from ±1.0 to ±0.70 in 0.05 e steps. We note that the original charges reproduce the experimental liquid density to well within 1% (ρ_{NPT} = 1.088 g cm^{-3}). As can clearly be seen, reduction of the atomic charges by a factor of 0.84/0.85 gives good agreement with the experimentally determined diffusion coefficients (Table 7) and possesses acceptable error in the calculated liquid density (around 3%). The effects on the other properties of the system from charge scalings of this magnitude are, on the whole, negligible—probability densities (not shown) and cation−anion coordination numbers (6.91 for the original forcefield, 7.12 for a charge scaling of 0.85) are almost unchanged between the two. The RDFs display a similar picture but with one subtle and important change in the cation−cation curve—the prepeak at 4 Å, indicative in the original results of cation stacking, is markedly decreased in the scaled charge model and is more consistent with the distributions determined from the neutron diffraction data. Log$_{10}$−log$_{10}$ plots of the mean squared displacement for cations and anions from the original charges and those scaled by a factor of 0.85 both show gradients close to 1 (see Supporting Information, Figure S2); therefore, the modeling is in the linear diffusive regime after 1 ns. Hence, the scaling of the charges is thought to be justified, and the calculated diffusion coefficients are reasonable.

Conclusions

This is the first ionic liquid structure investigation involving a polar, hydrogen-bonding, bidentate anion, with a directional

interaction to the cation, which allows extraction of more structural information than previous investigations. Similar probability distributions for cation−cation, cation−anion, and anion−anion densities are obtained using both approaches, EPSR simulation weighted to the experimentally determined liquid structure, and pure molecular dynamics simulations. The liquid structure of 1-ethyl-3-methylimidazolium acetate is as one would initially expect; i.e., the highest probability of anion density is associated with the three acidic hydrogens of the imidazolium ring. In common with [C$_1$mim]Cl which also contains a strongly hydrogen-bonding anion, this high probability of anion density in the cation plane results in a decrease in anion density above/below the ring, which then enables formation of aromatic cation−cation stacks—as observed by NMR. However, in comparison with [C$_1$mim]Cl, the first shell anion−cation RDF is much broader—being similar to that for [C$_1$mim][NTf$_2$] containing the much larger and poorly coordinating anion. This broad first coordination shell, which is significantly larger than the size of the acetate anion, combined with the observation of strong, directional H-bond interactions between the acetate carboxylate functions and the imidazolium cations leads to a model for the anion coordination shell being formed of acetate anions in approximately opposing orientations that result in the formation of a bilayer with a hydrophobic center comprised of methyl groups. The necessary formation of a Helmholtz electrostatic bilayer supports, nay, predicts and requires the formation of these structured anion regions in contrast to chlorides. The closest cation−anion contacts (within 3.7 Å) in [C$_2$mim][OAc] are found to be predominantly single contacts with relatively few bidentate, bridging, and bifurcated contacts. Diffusion coefficients of the ions have been determined by pulsed-field-gradient spin−echo NMR and are in agreement with the experiments of Moyna and co-workers[30] who suggest anion diffusion as part of larger ion aggregates.

Supporting Information Available: Normalized probabilities of dot products of cation *z*-axes (normal to ring plane) for cation pairs separated by between 3.2 and 4.6 Å and log$_{10}$−log$_{10}$ plots of mean squared displacement for cations and anions from the original charges and those scaled by a factor of 0.85. This material is available free of charge via the Internet at http://pubs.acs.org.

References and Notes

(1) Swatloski, R. P.; Spear, S. K.; Holbrey, J. D.; Rogers, R. D. *J. Am. Chem. Soc.* **2002**, *124*, 4974–4975.

(2) Pinkert, A.; Marsh, K. N.; Pang, S.; Staiger, M. P. Ionic Liquids and Their Interaction with Cellulose. *Chem. Rev.* **2009**, *109*, 6712–6728. Heinze, T.; Dorn, S.; Schöbitz, M.; Liebert, T.; Köhler, S.; Meister, F. Interactions of Ionic Liquids with Polysaccharides - 2: Cellulose. *Macromol. Symp.* **2008**, *262*, 8–22.

(3) Swatloski, R. P.; Spear, S. K.; Holbrey, J. D.; Rogers, R. D. *Abstr. Pap. Am. Chem. Soc.* **2002**, *224*, U622. Vanoye, L.; Fanselow, M.; Holbrey, J. D.; Atkins, M. P.; Seddon, K. R. *Green Chem.* **2009**, *11*, 390–396.

(4) Zhao, H. B.; Holladay, J. E.; Brown, H.; Zhang, Z. C. *Science* **2007**, *316*, 1597–1600. Moreau, C.; Finiels, A.; Vanoye, L. *J. Mol. Catal. A* **2006**, *253*, 165–169.

(5) Fukaya, Y.; Hayashi, K.; Wada, M.; Ohno, H. *Green Chem.* **2008**, *10*, 44–46.

(6) Zhang, Y.; Chan, J. Y. G. *Energy Environ. Sci.* **2010**, DOI: 10.1039/b914206a. Lee, S. H.; Doherty, T. V.; Linhardt, R. J.; Dordick, J. S. *Biotechnol. Bioeng.* **2009**, *102*, 1368–1376. Sun, N.; Rahman, M.; Qin, Y.; Maxim, M. L.; Rodríguez, H.; Rogers, R. D. *Green Chem.* **2009**, *11*, 646–655.

(7) Zhao, H.; Jackson, L.; Song, Z. Y.; Olubajo, A. *Tetrahetron: Asymmetry* **2006**, *17*, 2491–2498.

(8) Shiflett, M. B.; Yokozeki, A. *J. Chem. Eng. Data* **2009**, *54*, 108–114.

(9) Kiefer, J.; Obert, K.; Fries, J.; Bosmann, A.; Wasserscheid, P.; Leipertz, A. *Appl. Spectrosc.* **2009**, *63*, 1041–1049.

(10) Soper, A. K.; Howells, W. S.; Hannon, A. C. ATLAS-Analysis of Time-of-Flight Diffraction Data from Liquid and Amorphous Samples, Report RAL-89-046; Rutherford Appleton Laboratory, 1989.

(11) Holbrey, J. D.; Reichert, W. M.; Swatloski, R. P.; Broker, G. A.; Pitner, W. R.; Seddon, K. R.; Rogers, R. D. *Green Chem.* **2002**, *4*, 407–413.

(12) Soper, A. K. *Chem. Phys.* **1996**, *202*, 295–306. Soper, A. K. *Chem. Phys.* **2000**, *258*, 121–137. Soper, A. K. *Mol. Phys.* **2001**, *99*, 1503–1516.

(13) Gordon, M. S.; Schmidt, M. W.; Dykstra, C. E.; Frenking, G.; Kim, K. S.; Scuseria, G. E. *Theory and Applications of Computational Chemistry: the first forty years Advances in electronic structure theory: GAMESS a decade later*; Elsevier: Amsterdam, 2005; Vol. 116, pp 7−1189.

(14) Stejskal, E. O.; Tanner, J. E. *J. Chem. Phys.* **1965**, *42* (1), 288–292.

(15) Smith, W.; Leslie, M.; Forester, T. R. *DL POLY*, v2.17; Daresbury Laboratories, 2004.

(16) Canongia Lopes, J. N.; Padua, A. A. H. *J. Phys. Chem. B* **2004**, *108*, 16893–16898.

(17) Jorgensen, W. L.; Tirado-Rives, J. *Abst. Pap. Am. Chem. Soc.* **1998**, *216*, U696.

(18) Hardacre, C.; Holbrey, J. D.; McMath, S. E. J.; Bowron, D. T.; Soper, A. K. *J. Chem. Phys.* **2003**, *118*, 273–278.

(19) Hardacre, C.; McMath, S. E. J.; Nieuwenhuyzen, M.; Bowron, D. T.; Soper, A. K. *J. Phys.: Condens. Matter* **2003**, *15*, S159–S166.

(20) Deetlefs, M.; Hardacre, C.; Nieuwenhuyzen, M.; Padua, A. A. H.; Sheppard, O.; Soper, A. K. *J. Phys. Chem. B* **2006**, *110*, 12055–12061.

(21) Schröder, C.; Rudas, T.; Neumayr, G.; Gansterer, W.; Steinhauser, O. *J. Chem. Phys.* **2007**, *127*, 044505-1–044505-10.

(22) Avent, A. G.; Chaloner, P. A.; Day, M. P.; Seddon, K. R.; Welton, T. *J. Chem. Soc., Dalton Trans.* **1994**, *23*, 3405–3413.

(23) Hardacre, C.; Holbrey, J. D.; Nieuwenhuyzen, M.; Youngs, T. G. A. *Acc. Chem. Res.* **2007**, *40*, 1146–1155.

(24) Tokuda, H.; Hayamizu, K.; Ishii, K.; Susan, M. A. B. H.; Watanabe, M. *J. Phys. Chem. B* **2005**, *109*, 6103–6110.

(25) Noda, A.; Hayamizu, K.; Watanabe, M. *J. Phys. Chem. B* **2001**, *105*, 4603–4610.

(26) Tokuda, H.; Hayamizu, K.; Ishii, K.; Susan, M. A. B. H.; Watanabe, M. *J. Phys. Chem. B* **2004**, *108*, 16593–16600.

(27) Tokuda, H.; Ishii, K.; Susan, M. A. B. H.; Tsuzuki, S.; Hayamizu, K.; Watanabe, M. *J. Phys. Chem. B* **2006**, *110*, 2833–2839.

(28) Hayamizu, K.; Aihara, Y.; Nakagawa, H.; Nukuda, T.; Price, W. S. *J. Phys. Chem. B* **2004**, *108*, 19527–19532.

(29) Borodin, O.; Smith, G. D.; Henderson, W. *J. Phys. Chem. B* **2006**, *110*, 16879–16886.

(30) Remsing, R. C.; Hernandez, G.; Swatloski, R. P.; Massefski, W. W.; Rogers, R. D.; Moyna, G. *J. Phys. Chem. B* **2008**, *112*, 11071–11078.

(31) Chung, S. H.; Lopato, R.; Greenbaum, S. G.; Shirota, H. Jr.; Wishart, J. F. *J. Phys. Chem. B* **2007**, *111*, 4885–4893.

(32) Youngs, T. G. A.; Hardacre, C. *Chem. Phys. Chem.* **2008**, *9*, 1548–1558.